Generalized line tension of water nanodroplets

Matej Kanduč,[1,*] Laila Eixeres,[2] Susanne Liese,[3] and Roland R. Netz[2]
[1]*Research Group for Simulations of Energy Materials, Helmholtz-Zentrum Berlin für Materialien und Energie, Hahn-Meitner-Platz 1, 14109 Berlin, Germany*
[2]*Freie Universität Berlin, Fachbereich Physik, Arnimallee 14, 14195 Berlin, Germany*
[3]*Mechanics Section, Department of Mathematics, University of Oslo (UiO), P.O. Box 1053, Blindern, NO-0316 Oslo, Norway*

(Received 13 June 2018; published 28 September 2018)

We compare all-atom simulations of nanoscale water droplets of spherical and cylindrical morphologies on flat surfaces with tunable polarities. We find that for both morphologies, the contact angle depends, albeit differently, on the droplet size, which can be well described by the modified Young equation with an apparent line tension as a fitting parameter. In order to quantify the origin of the apparent line tension, we invoke a continuum-level description of the droplets for both morphologies. This enables us to decompose the apparent line tension into individual components that stem from a contact-angle dependent line tension and the Tolman correction to the surface tension.

DOI: 10.1103/PhysRevE.98.032804

I. INTRODUCTION

Wetting phenomena on solid surfaces are of high scientific and technological relevance with applications ranging from microfluidics and nanofluidics to nanomaterial engineering [1–4]. Water is of particular interest in wetting studies, as it represents a common liquid in many industrial processes such as dyeing, coating, painting, lubrication, oil recovery, and deposition of pesticides [5]. When a water drop is deposited on a solid surface, two distinct behaviors are possible: partial wetting, where the drop forms a finite contact angle θ with the surface, or complete wetting, with vanishing contact angle ($\theta = 0$) [6]. In the former case, the contact angle θ_0 that a macroscopic water drop (i.e., large compared with the range of intermolecular forces, surface asperities, and chemical heterogeneities) forms with the surface is given by the well-known Young equation

$$\cos\theta_0 = \frac{\gamma_{sv} - \gamma_{sw}}{\gamma}, \tag{1}$$

and we will refer to it as a *macroscopic contact angle*. Here, γ_{sv}, γ_{sw}, and γ stand, respectively, for the surface-vapor, surface-water, and water-vapor surface tensions.

When droplets are of nanoscopic size, effects at the nanometer scale notably contribute to their form, and their contact angle θ can considerably differ from θ_0. Commonly, the contact angle dependence on the droplet size can be well described by the modified Young equation [7,8]

$$\cos\theta = \cos\theta_0 - \frac{\tau_{app}}{\gamma a}. \tag{2}$$

Here, a is the base radius of the droplet (Fig. 1) and τ_{app} stands for the *apparent line tension*. Note that the modified Young equation is originally based on the concept of line tension τ as the free energy correction produced by the contact line where the three phases meet [9]. The assumption that τ is independent of the droplet's geometry (e.g., the contact angle) and that it is the sole correction contribution at the nanoscopic scale, leads to the original version of the modified Young equation where τ replaces τ_{app} in Eq. (2) [9]. But due to additional effects that in many cases contribute to the contact angle, the parameter τ_{app} obtained from a fit of Eq. (2) to experimental [10–14] or simulation [15–18] data cannot be considered as the line tension τ in terms of the excess free energy of the contact line. Instead, the apparent line tension τ_{app} is an effective parameter that clumps together all the contributions of the size dependence of the contact angle. In this paper, we therefore strictly distinguish between the line tension, defined within a continuum description as the excess free energy (dW) per unit length of a contact line (dL), $\tau = dW/dL$, and the apparent line tension τ_{app}, which is the fitting parameter defined in Eq. (2).

The contact line is a key player in the stability of droplets, liquid deposits of various morphologies, and also of films, foams, and nanobubbles, because it decisively contributes to the free energy of nanoscopic wetting scenarios [19–24]. Thus, distinguishing between τ and τ_{app}, along with the knowledge on additional contributions to the free energy, are crucial for understanding wetting processes.

In this study, we compare results from atomistic simulations of spherical and cylindrical water droplets on flat and chemically uniform surfaces of different polarities. We compare our simulation results with a continuum approach based on free energy minimization that enables us to decompose the apparent line tension in to three contributions: the line tension, the line tension stiffness, and the Tolman contribution.

II. METHODS

We perform molecular dynamics (MD) simulations of spherical droplets [Fig. 1(a)] on flat surfaces and compare

*matej.kanduc@helmholtz-berlin.de

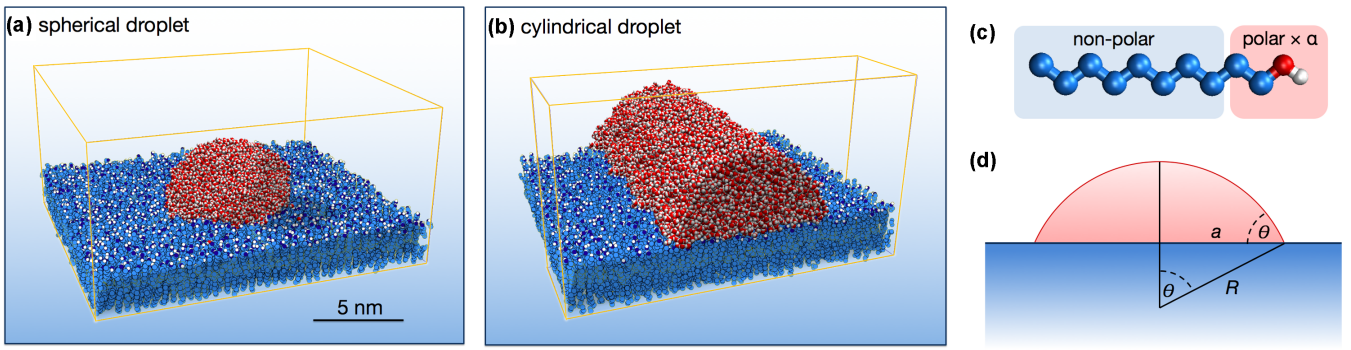

FIG. 1. Snapshots of the simulation setups: (a) a spherical and (b) a cylindrical water droplet (simulation data from Ref. [25]) on the surface with polarity $\alpha = 0.6$. (c) A surface molecule is composed of an aliphatic chain terminated by a modified hydroxyl group whose polarity is rescaled by a factor α. (d) A cross section of the droplet with a radius of curvature R and a base radius a forming a contact angle θ with the surface.

them with the results of cylindrical droplets [Fig. 1(b)] on the same surfaces from our previous study [25]. In order to do this, we use the same simulation model and closely follow the methods of Ref. [25], which we now briefly recap. The planar surface is composed of anchored hexagonally arranged aliphatic chains terminated by hydroxyl (OH) head groups [Fig. 1(c)] with an area density of 4.3 nm^{-2}. The surface polarity, and by that the water adhesion strength, is tuned by scaling the partial charges of the head groups by a polarity parameter α in the range between 0 and 0.83. The simulation box of lateral dimensions 18 nm $\times$ 21 nm and height 10 nm is replicated in all three directions via periodic boundary conditions. The water droplets deposited on the surface consist of 800 to 4600 water molecules, initially in the form of a cuboid, which rapidly equilibrate to a spherical form [Fig. 1(a)].

We utilize the united-atom GROMOS force field [26] for the surface molecules and the simple point charge/extended (SPC/E) water model [27]. The MD simulations were performed with the GROMACS simulation package [28] in the canonical (NVT) ensemble. The system temperature is maintained at 300 K by the velocity-rescaling thermostat [29] with a time constant of 0.1 ps [30]. Electrostatics is treated using particle-mesh-Ewald methods [31,32] with a real-space cutoff of 0.9 nm. The LJ potentials are cut off at 0.9 nm.

The simulation times span from 250 to 500 ns. The limiting factor in the equilibration is the formation of a sub-monolayer water film, which evolves by the diffusion of water molecules from the droplet to the rest of the surface. The thickness and other characteristics of this water film were analyzed elsewhere [33]. On hydrophobic surfaces, where the thickness of the water film is negligible, the droplets equilibrate in less than 1 ns. On the other hand, the formation of equilibrium water films on hydrophilic surfaces can take up to 100 ns. Contact-line pinning and contact-angle hysteresis have negligible effects on the equilibrium shape of the droplet in this model [25]. After equilibration, the radial density profile of water is used to identify an effective water-vapor interface (defined as the Gibbs dividing surface) as outlined in similar studies [15,25,34–38]. Likewise, the effective water-surface interface is defined as the Gibbs dividing surface of the water phase from independent simulations of the surface in contact with a bulk water slab [25]. The effective interfacial shape of the droplet is then fitted with a spherical cap, from which the base radius a and the contact angle θ with the surface [Fig. 1(d)] are obtained.

III. RESULTS AND DISCUSSION

A. Spherical vs cylindrical droplets

Plotting the cosine of the measured contact angles $\cos\theta$ versus the inverse base radius $1/a$ [Fig. 2(a)] reveals a clear linear relationship for all surface polarities. The data have been shifted by the extrapolated values of $\cos\theta_0$, such that the linear fits (see below) merge at $1/a = 0$ (except for $\alpha = 0.6$ and 0.7, which are shifted vertically by 0.05 and 0.1, respectively, for better clarity). The MD data points can be well fitted with the modified Young equation, Eq. (2), as indicated by solid lines in Fig. 2(a). The obtained macroscopic contact angle θ_0 on the completely non-polar surface ($\alpha = 0$) is 134° [Fig. 2(b)], it monotonically decreases with surface polarity, and above around $\alpha = 0.85$ the surface enters the regime of complete wetting, where $\theta_0 = 0$.

The relation between the measured apparent line tension τ_{app} [as defined in Eq. (2)] and $\cos\theta_0$ for the spherical droplets is shown in Fig. 2(c) by orange circles. For hydrophobic and weakly hydrophilic surfaces τ_{app} is negative, but becomes positive for very hydrophilic surfaces (for $\cos\theta_0 > 0.8$ or $\theta_0 < 35°$). This means that except for very hydrophilic surfaces, small droplets have a smaller contact angle than macroscopic drops, as is also evident from the scaling plot in Fig. 2(a).

In Fig. 2(c), we additionally present the results of cylindrical droplets [Fig. 1(b)] by blue square symbols on identical surfaces from Ref. [25]. Note that in that study, the scaling of the contact angle with the droplet size was expressed in terms of the droplet's curvature $1/R$ as $\cos\theta = \cos\theta_0 + C/R$. In order to compare this relation to Eq. (2), we associate the coefficient C with the apparent line tension as $\tau_{\mathrm{app}}^{\mathrm{cyl}} = -C\gamma\sin\theta_0$, where we used the geometric relation $\sin\theta_0 = a/R$. The values of $\tau_{\mathrm{app}}^{\mathrm{cyl}}$ for the cylindrical droplets are significantly smaller in magnitude than τ_{app} for the spherical droplets. This means that the contact angles of cylindrical droplets are much less sensitive to the droplet size than spherical droplets. Yet, the qualitative behavior is similar: Negative apparent line tension on hydrophobic and weakly hydrophilic surfaces, and positive on very hydrophilic surfaces. This result partially

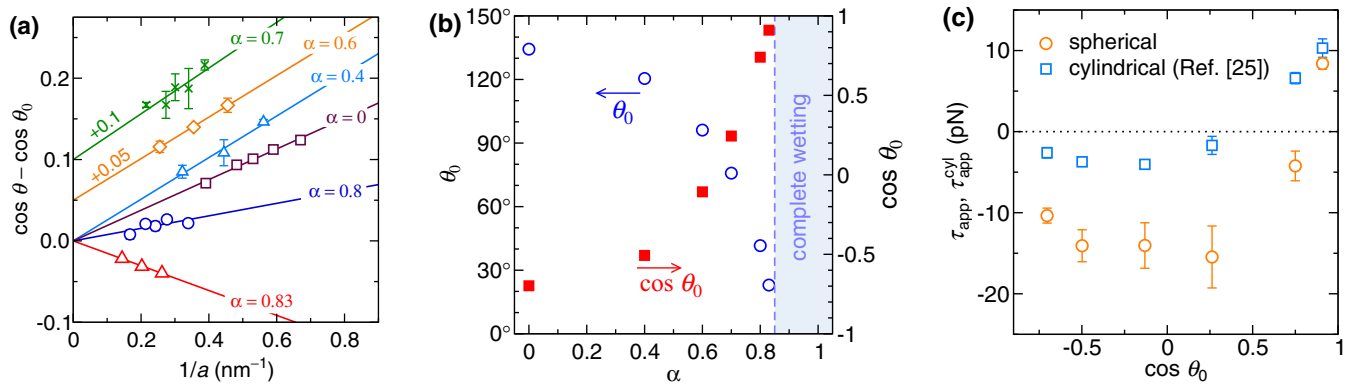

FIG. 2. (a) The cosine of the measured droplet contact angles (shifted by $\cos\theta_0$) versus the inverse base radius $1/a$ of the spherical droplet. The data for $\alpha = 0.6$ and 0.7 are shifted vertically by 0.05 and 0.1, respectively, for better visibility. The solid lines are fits of Eq. (2) to the MD data points. (b) Macroscopic contact angle (left scale) and its cosine (right scale) obtained from the fits of Eq. (2) to the data points in (a). The error bars are around $\delta\theta \sim 1^\circ$ and thus smaller than the symbols. (c) Evaluated apparent line tension from the spherical droplets, $\tau_{\rm app}$, (a) and cylindrical droplets, $\tau_{\rm app}^{\rm cyl}$, (adopted from Ref. [25]).

supports the common practice to use the cylindrical morphology in computer simulations to reduce the effect of line tension [33,36,39–41]. Even though the size-scaling effects on the droplets are weaker in the cylindrical morphology, they do not entirely vanish. Similar conclusions were reported also for graphene layers by Scocchi *et al.* [42]. On the other hand, simulations of cylindrical droplets composed of a Lennard-Jones fluid did not demonstrate significant size-dependent contact angles [35,43,44]. So, we conclude that even cylindrical droplets show finite-size effects, which depend on the type of the liquid.

B. Decomposition of the apparent line tension

In order to interpret the simulation results in Fig. 2(c) from a theoretical point of view, we invoke a continuum-level description of the droplet based on the minimization of its free energy.

An important effect that has to be taken into account stems from the curved water-vapor interface of the droplet. The curvature correction to the surface tension $\gamma(R)$ is to lowest order expressed as [45]

$$\gamma(R) = \gamma\left(1 - \frac{2\delta_{\rm T}}{R}\right), \tag{3}$$

where γ is the surface tension of the flat interface, R the radius of curvature, and $\delta_{\rm T}$ the *Tolman length* [46].

At the same time, the contribution of the three-phase contact line is taken into account by introducing the *line tension* as the excess free energy per unit length of the contact line. As it turns out, the assumption of a constant line tension that is independent of the geometry of the contact line cannot describe our results. Therefore, we postulate a "generalized" line tension $\tau(\theta)$ that is an explicit function of the contact angle θ at *fixed* thermodynamic conditions. This concept has been introduced in various theoretical studies, since the molecular interactions at the three-phase contact line obviously depend on the local geometry, that is, also on the contact angle [7,47–51].

So far, no consensus exists regarding the functional dependence of $\tau(\theta)$. For this reason, we express $\tau(\theta)$ in the form of a Taylor expansion around the macroscopic limit

$$\tau(\theta) = \tau_0 + \tau_1(\theta - \theta_0) + \ldots. \tag{4}$$

Here, τ_0 is the line tension of the macroscopic drop (i.e., with $\theta = \theta_0$), which we refer to as the *macroscopic line tension*. The second term represents the first-order correction to the line tension due to the deviation of the contact angle θ from the macroscopic value θ_0. The coefficient $\tau_1 = {\rm d}\tau(\theta)/{\rm d}\theta$ has been termed *line tension stiffness* [51] as it can be interpreted as a "stiffness" of the line tension against contact angle variation at fixed thermodynamic conditions. In this manner, τ_1 is an additional parameter that, together with τ_0, characterizes the generalized line tension $\tau(\theta)$. Both τ_0 and τ_1 in general depend on the surface polarity (thus on θ_0) but are by construction independent of θ. Higher-order terms in Eq. (4) will be neglected in our analysis.

As suggested in the literature [51], the generalized line tension can also depend on the curvature of the contact line, hence $\tau(a,\theta)$. Analogously to the Tolman correction in Eq. (3) for the surface tension, we expect an asymptotic correction of the order of $\sim 1/a$ for the line tension. However, such a correction would yield a size-independent term in the free energy [see below, Eq. (5)] and would not contribute to the size scaling. Only the next-leading term $\sim 1/a^2$ in $\tau(a,\theta)$ would contribute, but that already corresponds to a correction in the free energy two orders higher than we consider in our analysis.

Using the above assumptions, we now express the free energy of the spherical droplet as

$$W = A_{\rm cap}\gamma(R) - A_{\rm base}(\gamma_{\rm sv} - \gamma_{\rm sw}) + 2\pi a\tau(\theta). \tag{5}$$

The first term corresponds to the free energy of the water-vapor interface, which has the shape of a spherical cap with the surface area $A_{\rm cap} = 2\pi R^2(1 - \cos\theta)$. The second term is the free energy of the interface between the droplet's base and the surface, with the area $A_{\rm base} = \pi a^2$. The last term is the excess free energy of the circular three-phase contact line

of length $2\pi a$, characterized by the line tension $\tau(\theta)$ given by Eq. (4).

The equilibrium contact angle θ and the base radius a of the droplet follow from the minimization of the free energy W at fixed volume of the droplet, which is given by

$$V = \frac{\pi}{3} R^3 (2 - 3\cos\theta + \cos^3\theta). \tag{6}$$

The problem can be solved by using the method of Lagrange multipliers. This requires the minimization of the function

$$w = W - \lambda V \tag{7}$$

with respect to θ and a, which yields the equations $\partial w/\partial\theta = 0$ and $\partial w/\partial a = 0$. After eliminating the Lagrange multiplier λ from both equations, we obtain the expression that relates θ and a,

$$\cos\theta = \cos\theta_0 - \frac{\tau_0}{\gamma a} + \frac{(2+\cos\theta)\sin\theta}{\gamma a}\tau_1 - \frac{(\theta-\theta_0)\tau_1}{\gamma a} - \frac{2\delta_T}{a}\sin\theta. \tag{8}$$

Here, we have expressed $\gamma_{sv} - \gamma_{sw}$ by the macroscopic contact angle θ_0 given by Eq. (1).

Equation (8) can be further simplified by replacing θ by θ_0 in all correction terms on the right-hand side that scale as $1/a$. With this, we recover the generic form of the modified Young equation [Eq. (2)] by defining the apparent line tension as

$$\tau_{app} = \tau_0 - \tau_1(2+\cos\theta_0)\sin\theta_0 + 2\gamma\delta_T\sin\theta_0. \tag{9}$$

This result shows that the apparent line tension is an outcome of several effects, in particular the line tension that depends on the contact angle [Eq. (4)]. A similar decomposition of the apparent line tension was suggested by Schimmele *et al.* [51] but based on slightly different definitions of the line tension and its components.

Going back to Eq. (5), we see that the first two terms, which scale with the droplet surface area ($\sim a^2$) and thus represent the dominant contributions to the free energy, contribute to the value of $\cos\theta_0$. On the other hand, the line tension as well as the Tolman correction [the latter being characterized by $\gamma(R)$] contribute only linearly ($\sim a$) and hence represent next-to-leading contributions, which are manifested in τ_{app} [Eq. (9)]. Postulating even higher-order corrections to the free energy (not included in our analysis) would result in an a-dependent τ_{app}. However, the MD data in Fig. 2(a) can be well fitted by Eq. (2) with an a-independent τ_{app}, thus we conclude that for our droplet sizes $a > 2$–3 nm ($1/a < 0.3$–0.5 nm^{-1}) higher-order corrections to Eq. (5) are negligible.

Clearly, only by measuring the contact-angle dependence on the droplet size, one cannot access the individual components in Eq. (9), but only their sum, τ_{app}.

Likewise, for the cylindrical morphology, the same theoretical framework as used in Eq. (5) (see Ref. [25] for details) yields the following expression for the apparent line tension:

$$\tau_{app}^{cyl} = (\tau_1 - \gamma\delta_T)\left(\frac{\theta_0 - \sin\theta_0\cos\theta_0}{\theta_0\cos\theta_0 - \sin\theta_0}\right)\sin\theta_0. \tag{10}$$

Note that τ_0 does not enter this relation, since the length of the contact line in a cylindrical droplet does not change with θ.

We now analyze the MD simulation results of both spherical and cylindrical water droplets [Fig. 2(c)] in terms of Eqs. (9) and (10), which allows us to determine the parameters γ, δ_T, τ_0, and τ_1. As opposed to τ_0 and τ_1, the parameters γ and δ_T depend only on the water model and not on the surface parameters. The flat water-vapor surface tension of the SPC/E water $\gamma = 55$ mN/m is easily accessible from a simulation of a water slab in a vapor phase from the diagonal pressure tensor components [25,52]. On the other hand, the value of the Tolman length for water was debated in the literature [53–55]. In this study, we adopt the value $\delta_T = -0.05$ nm that we obtained for the SPC/E water model in our previous study [25]. There, δ_T was computed from the tensile force of a water cylinder spanning across the simulation box with periodic boundary conditions. This value also agrees well with recent experimental [56] and theoretical [25,57–59] studies. A negative Tolman length favors water cavities over droplets, tends to flatten the droplet, and thus yields a negative contribution to τ_{app} in Eq. (9).

Once γ and δ_T are resolved, we use τ_{app}^{cyl} data for cylindrical droplets [Fig. 2(c)] to obtain τ_1 from Eq. (10). The evaluated values of τ_1 are shown by triangles in Fig. 3(a). Finally, the remaining parameter τ_0 can now be calculated from τ_{app} values for the spherical droplets via Eq. (9) [shown by square symbols in Fig. 3(a)].

After all the parameters have been determined, we can now decompose the measured τ_{app} of the spherical droplet into the

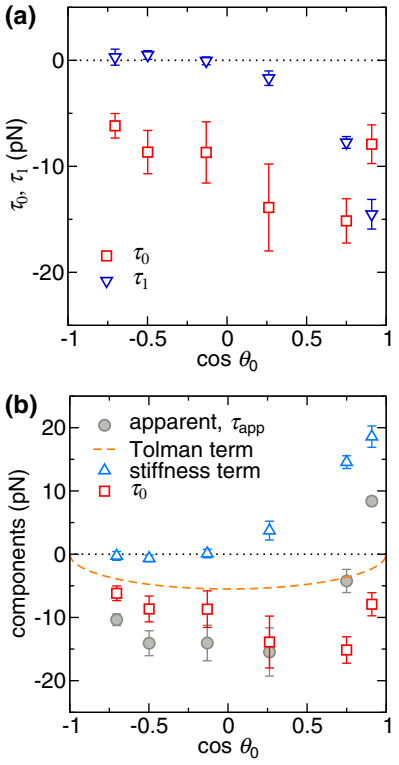

FIG. 3. (a) The macroscopic line tension τ_0 and the line tension stiffness τ_1 [as defined in Eq. (4)]. (b) Decomposition of the apparent line tension τ_{app} of the spherical droplet to the three components according to Eq. (9): the Tolman term ($2\gamma\delta_T\sin\theta_0$), the angle-stiffness term [$-\tau_1(2+\cos\theta_0)\sin\theta_0$], and the macroscopic line tension τ_0.

components defined in Eq. (9), as shown in Fig. 3(b). The Tolman contribution [the third term in Eq. (9)] scales as $\sim \sin\theta_0$ and is therefore vanishing for very hydrophilic and very hydrophobic surfaces. The stiffness coefficient τ_1 [Fig. 3(a)] is negligible for hydrophobic surfaces, but becomes significant on hydrophilic surfaces. The resulting stiffness contribution to τ_{app} [the second term in Eq. (9)] correspondingly is negligible for hydrophobic surfaces, but represents a dominant contribution for hydrophilic surfaces [triangle symbols in Fig. 3(b)]. Finally, the macroscopic line tension, τ_0, (shown by red squares) is negative on the entire range of surface polarities.

This analysis demonstrates that all three terms in Eq. (9) are comparable in magnitude, which is of the order of 10 pN. This order of magnitude has been reported also in various experimental and theoretical works [12,15,16,51,60–62] for flat and chemically homogeneous surfaces. In fact, it corresponds to the typical strength of intermolecular forces in water, which can be estimated as $\gamma d \approx 20$ pN (with $d \approx 0.3$ nm being the size of the water molecule).

The contact angles of the droplets in our simulations for a given surface polarity differ among each other by less than $|\theta - \theta_0| < 4^\circ$ [cf. Fig. 2(a)]. This means that the line tension $\tau(\theta)$ [Eq. (4)] is governed by the leading-order term, $\tau(\theta) \simeq \tau_0$, and does not differ significantly among the droplets of different sizes. But interestingly, the contact angle dependence of $\tau(\theta)$, characterized by the stiffness coefficient τ_1, generates a significant contribution to the apparent line tension τ_{app}. For very polar surfaces ($\alpha = 0.83$), the contribution due to the stiffness becomes dominant and even engenders a positive apparent line tension $\tau_{\text{app}} > 0$, while the line tension is negative $\tau(\theta) \simeq \tau_0 < 0$.

IV. CONCLUSIONS

We compare all-atom simulations of nano-scale water droplets of spherical and cylindrical morphologies on various polar flat surfaces. In both morphologies, the contact angle depends significantly on the droplet size and can be well described by the modified Young equation with the apparent line tension τ_{app} as a fitting parameter. In order to interpret the simulation results, we use a continuum-level description of the droplets where we assume the contributions to the free energy from the Tolman correction of the curved water-vapor interface and a generalized line tension $\tau(\theta)$ that is a function of the contact angle. The latter functional dependence we describe by the stiffness coefficient τ_1 that corresponds to the derivative of the line tension with respect to the contact angle.

The simulation results from both morphologies enable us to evaluate the line tension and its stiffness contribution for the given atomistic model. We find a strictly negative line tension, $\tau(\theta) \approx \tau_0 < 0$, for all surface polarities [Fig. 3(c)]. However, the apparent line tension τ_{app} can significantly deviate from the line tension $\tau(\theta)$ and it even becomes positive on very hydrophilic surfaces due to a considerable stiffness component.

An important conclusion that transpires from our analysis is that the nature of the line tension considerably influences the contact angle and probably other wetting phenomena as well. However, most theoretical studies do not consider the dependence of the (generalized) line tension on the droplet geometry, even though we demonstrate it to be crucial for understanding of nanoscale phenomena. The concept of the generalized line tension is expected to be particularly relevant for hydrophilic surfaces, where we find a large stiffness coefficient. On the other hand, the phenomena on non-polar surfaces, such as the stability of air nanobubbles [62], are expected to be less affected. The details of the line tension are determined by surface-liquid molecular interactions, which can be expressed also in terms of an interface potential (or its negative derivative, the disjoining pressure) [63]. In fact, the interface potential contains all necessary information for evaluating the line tension of the system [64,65], which is an interesting matter to be verified with atomistic models.

Note that in general also other effects can contribute to the apparent line tension, stemming for instance from surface roughness, chemical heterogeneities, and impurities [24,47,50,51,60,66,67]. The subtle nature of the line tension and ambiguities in its exact definition are a source of wide discrepancies in its measured values, spanning over several orders of magnitude [24,51,68]. For a proper understanding of numerous wetting processes, it is thus of vital importance to identify and to understand the individual components that contribute to the nature of the three-phase contact line.

ACKNOWLEDGMENTS

Funding by the Deutsche Forschungsgemeinschaft (DFG) via Grant No. NE 810/11 is gratefully acknowledged.

[1] D. Bonn, J. Eggers, J. Indekeu, J. Meunier, and E. Rolley, Rev. Mod. Phys. **81**, 739 (2009).
[2] R. Seemann, M. Brinkmann, E. J. Kramer, F. F. Lange, and R. Lipowsky, Proc. Natl. Acad. Sci. **102**, 1848 (2005).
[3] A. Méndez-Vilas, A. B. Jódar-Reyes, and M. L. González-Martín, Small **5**, 1366 (2009).
[4] D. Lohse, X. Zhang *et al.*, Rev. Mod. Phys. **87**, 981 (2015).
[5] A. Rosenhahn, S. Schilp, H. J. Kreuzer, and M. Grunze, Phys. Chem. Chem. Phys. **12**, 4275 (2010).
[6] P. G. de Gennes, Rev. Mod. Phys. **57**, 827 (1985).
[7] L. Boruvka and A. Neumann, J. Chem. Phys. **66**, 5464 (1977).
[8] J. Gaydos and A. Neumann, Adv. Colloid Interface Sci. **120**, 76 (1987).
[9] J. W. Gibbs, *The Scientific Papers* (Dover, New York, 1961), Vol. I.
[10] J. Y. Wang, S. Betelu, and B. M. Law, Phys. Rev. Lett. **83**, 3677 (1999).
[11] F. Mugele, T. Becker, R. Nikopoulos, M. Kohonen, and S. Herminghaus, J. Adhes. Sci. Technol. **16**, 951 (2002).
[12] J. K. Berg, C. M. Weber, and H. Riegler, Phys. Rev. Lett. **105**, 076103 (2010).
[13] D. A. Leelamanie and J. Karube, Soil Sci. Plant Nutr. **58**, 675 (2012).
[14] L.-O. Heim and E. Bonaccurso, Langmuir **29**, 14147 (2013).
[15] T. Werder, J. H. Walther, R. L. Jaffe, T. Halicioglu, and P. Koumoutsakos, J. Phys. Chem. B **107**, 1345 (2003).

[16] G. Yiapanis, S. Maclaughlin, E. J. Evans, and I. Yarovsky, Langmuir **30**, 10617 (2014).
[17] M. Khalkhali, N. Kazemi, H. Zhang, and Q. Liu, J. Chem. Phys. **146**, 114704 (2017).
[18] M. H. Anvari, Q. Liu, Z. Xu, and P. Choi, J. Mol. Liq. **248**, 634 (2017).
[19] R. Rosso and E. G. Virga, Phys. Rev. E **70**, 031603 (2004).
[20] M. Brinkmann, J. Kierfeld, and R. Lipowsky, J. Phys. A **37**, 11547 (2004).
[21] M. Brinkmann, J. Kierfeld, and R. Lipowsky, J. Phys. Condens. Matter **17**, 2349 (2005).
[22] L. Guzzardi, R. Rosso, and E. G. Virga, Phys. Rev. E **73**, 021602 (2006).
[23] J. Zhang, M. K. Borg, K. Ritos, and J. M. Reese, Langmuir **32**, 1542 (2016).
[24] B. M. Law, S. P. McBride, J. Y. Wang, H. S. Wi, G. Paneru, S. Betelu, B. Ushijima, Y. Takata, B. Flanders, F. Bresme *et al.*, Prog. Surf. Sci. **92**, 1 (2017).
[25] M. Kanduč, J. Chem. Phys. **147**, 174701 (2017).
[26] C. Oostenbrink, A. Villa, A. E. Mark, and W. F. van Gunsteren, J. Comput. Chem. **25**, 1656 (2004).
[27] H. J. C. Berendsen, J. R. Grigera, and T. P. Straatsma, J. Phys. Chem. **91**, 6269 (1987).
[28] D. van der Spoel, E. Lindahl, B. Hess, G. Groenhof, A. E. Mark, and H. J. C. Berendsen, J. Comput. Chem. **26**, 1701 (2005).
[29] G. Bussi, D. Donadio, and M. Parrinello, J. Chem. Phys. **126**, 014101 (2007).
[30] H. J. C. Berendsen, J. P. M. Postma, W. F. van Gunsteren, A. DiNola, and J. R. Haak, J. Chem. Phys. **81**, 3684 (1984).
[31] T. Darden, D. York, and L. Pedersen, J. Chem. Phys. **98**, 10089 (1993).
[32] U. Essmann, L. Perera, M. L. Berkowitz, T. Darden, H. Lee, and L. G. Pedersen, J. Chem. Phys. **103**, 8577 (1995).
[33] M. Kanduč and R. R. Netz, J. Chem. Phys. **146**, 164705 (2017).
[34] M. J. de Ruijter, T. Blake, and J. De Coninck, Langmuir **15**, 7836 (1999).
[35] J. H. Weijs, A. Marchand, B. Andreotti, D. Lohse, and J. H. Snoeijer, Phys. Fluids **23**, 022001 (2011).
[36] D. Vanzo, D. Bratko, and A. Luzar, J. Chem. Phys. **137**, 034707 (2012).
[37] H. Peng, A. V. Nguyen, and G. R. Birkett, Mol. Simul. **38**, 945 (2012).
[38] J. Zhang, F. Leroy, and F. Müller-Plathe, Langmuir **29**, 9770 (2013).
[39] J. Driskill, D. Vanzo, D. Bratko, and A. Luzar, J. Chem. Phys. **141**, 18C517 (2014).
[40] F. Leroy, J. Chem. Phys. **145**, 164705 (2016).
[41] H. Jiang, F. Müller-Plathe, and A. Z. Panagiotopoulos, J. Chem. Phys. **147**, 084708 (2017).
[42] G. Scocchi, D. Sergi, C. D'Angelo, and A. Ortona, Phys. Rev. E **84**, 061602 (2011).
[43] H. Peng, G. R. Birkett, and A. V. Nguyen, Mol. Simul. **40**, 934 (2014).
[44] J. Zhang, F. Leroy, and F. Müller-Plathe, Phys. Rev. Lett. **113**, 046101 (2014).
[45] A. van Giessen, E. Blokhuis, and D. J. Bukman, J. Chem. Phys. **108**, 1148 (1998).
[46] R. C. Tolman, J. Chem. Phys. **17**, 333 (1949).
[47] A. Marmur, J. Colloid Interface Sci **186**, 462 (1997).
[48] Y. Solomentsev and L. R. White, Adv. Colloid Interface Sci. **218**, 122 (1999).
[49] A. Marmur and B. Krasovitski, Langmuir **18**, 8919 (2002).
[50] A. Rusanov, A. Shchekin, and D. Tatyanenko, Colloids Surf., A **250**, 263 (2004).
[51] L. Schimmele, M. Napiórkowski, and S. Dietrich, J. Chem. Phys. **127**, 164715 (2007).
[52] M. J. P. Nijmeijer, C. Bruin, A. F. Bakker, and J. M. J. van Leeuwen, Phys. Rev. A **42**, 6052 (1990).
[53] Y. A. Lei, T. Bykov, S. Yoo, and X. C. Zeng, J. Am. Chem. Soc. **127**, 15346 (2005).
[54] A. J. Castellanos S, J. Toro-Mendoza, and M. Garcia-Sucre, J. Phys. Chem. B **113**, 5891 (2009).
[55] F. Sedlmeier and R. R. Netz, J. Chem. Phys. **137**, 135102 (2012).
[56] M. E. M. Azouzi, C. Ramboz, J.-F. Lenain, and F. Caupin, Nat. Phys. **9**, 38 (2013).
[57] M. N. Joswiak, N. Duff, M. F. Doherty, and B. Peters, J. Phys. Chem. Lett. **4**, 4267 (2013).
[58] Ø. Wilhelmsen, D. Bedeaux, and D. Reguera, J. Chem. Phys. **142**, 171103 (2013).
[59] M. N. Joswiak, R. Do, M. F. Doherty, and B. Peters, J. Chem. Phys. **145**, 204703 (2016).
[60] A. Amirfazli and A. Neumann, Adv. Colloid Interface Sci. **110**, 121 (2004).
[61] B. Lefevre, A. Saugey, J.-L. Barrat, L. Bocquet, E. Charlaix, P.-F. Gobin, and G. Vigier, J. Chem. Phys. **120**, 4927 (2004).
[62] L. Guillemot, T. Biben, A. Galarneau, G. Vigier, and É. Charlaix, Proc. Natl. Acad. Sci. **109**, 19557 (2012).
[63] N. Churaev and V. Sobolev, Adv. Colloid Interface Sci. **61**, 1 (1995).
[64] J. Indekeu, Phys. A **183**, 439 (1992).
[65] H. Dobbs and J. Indekeu, Phys. A **201**, 457 (1993).
[66] J. Drelich, J. D. Miller, and R. J. Good, Adv. Colloid Interface Sci. **179**, 37 (1996).
[67] D. Li, Colloids Surf., A **116**, 1 (1996).
[68] J. Drelich, Colloids Surf., A **116**, 43 (1996).